Turk J Elec Engin, VOL.16, NO.2 2008, © TÜBİTAK

Method of Moments Solution by Using Sinc-Type Basis Functions for the Scattering from a Finite Number of Conducting Strip Gratings

Taner OĞUZER[1], **Fadıl KUYUCUOĞLU**[2]
[1]*Electrical and Electronics Eng. Dept., Dokuz Eylül University, Buca, 35160 İzmir-TURKEY*
e-mail: taner.oguzer@deu.edu.tr
[2]*Electrical and Electronics Eng. Dept., Ege University, Bornova, 35100 İzmir-TURKEY*
e-mail: fadil_kuyu@hotmail.com

Abstract

A numerical method of moments (MoM) solution is applied to the electromagnetic scattering from a periodic finite conducting strip array when the incident electromagnetic plane wave E and H polarizations illuminate the grating. For such grating strip geometry, we deal with singular integral equations arising from Neumann and Dirichlet boundary conditions. MoM is applied using band-limited sinc functions as basis and testing functions. The Galerkin approach is followed in MoM formulation. The properties of the sinc function, with the infinite integral, are exploited in the computations of the main matrix elements. Also, the error in our approach goes to zero with increasing bandwidth or lower sampling rate. Results of our formulation are given as surface current densities and far field scattered data. Our data is also compared with previous results available in the literature.

1. Introduction

Electromagnetic scattering from strip geometries has been a great challenge for many years. Many researchers focused on infinite number of strips, particularly in periodic structures. Various analytical and numerical studies have been reported regarding this geometry for perfectly conducting and resistive type strips in free space or on a grounded slab. The resistive strip grating [1] is usually solved by the Spectral-Galerkin procedure. The Method of Moments (MoM) [2] is also used to solve for the Electric Field Integral Equation (EFIE) describing the behavior of the strips. Perfectly conducting and resistive strips were used to model the grounded dielectric slab geometry.

Recent advances in short pulse generation and processing have stimulated interest in wideband (WB) and ultra-wideband phenomena. In [3], an efficient technique has been developed for the analysis and numerical calculation of the ultra-wideband scattering from a finite array strips in free space. Later in [4], the geometry of the resistive strips on the grounded dielectric slab was solved by improving the technique presented in [3]. Also in [5], the absorption analysis of a strip grating placed on an absorber is studied utilizing MoM. In [6], numerical results are provided based on a full-wave moment-method discretization of

the relevant EFIE in the unit cell with an arbitrary phase shift between adjacent cells. This original MoM technique is utilized in [6] for the analysis of linear phased arrays of microstrip leaky-wave antennas.

For double strips in [7] and [8], Wiener-Hopf's technique is applied; but it is known that the asymptotic solutions are effective at high frequencies. As for frequencies where strips are narrower than wavelength, a quasi-static solution can be obtained as in [9]. An important alternative is to apply analytical technique in addition to numerical techniques, where the singular integral equation is converted and reduced to Fredholm second kind regular matrix [11]. For instance, various strip configurations in free space are analyzed by Veliev [17]. Here, the accuracy is increased but due to the time forming the main matrix elements, the cpu time of the overall solution is not reduced greatly.

In [10], a pure numerical solution is carried out at resonance, where the inverted matrix is too large, making it difficult to apply three or more strips efficiently due to limited memory storage and CPU time. The MoM procedure is applied in [15] using the closed form generalized Green's functions, as well as the generalized pencil-of-function method (GPOF), is applied to layered dielectric media. Free space results is investigated in [16]. In our investigation, we choose sinc-type basis functions for the method of moments. The sinc-type functons is widely used in a variety of cases, as shown in [12, 13]. For example, Recently, Hallen integral equation [14] is solved via the sinc collocation method. We use here the sinc collocation following the moment method procedure. Also the presented approach is applied to the singular EFIE as an example and we immensely benefited from the properties of the sinc functions [18].

Sinc functions have the property that the convolution of two sinc functions, at different locations, is a sinc function located at the point of the difference between the two. Therefore the convolution can be computed from a simple substitution and scalar multiplication. The procedure is similar to the sampling the surface current on the scatterer by using the sinc type interpolation. Then the integral of the Green's function, i.e. Hankel function, also with the sinc function appears in the same integrand is carried out at a specified point. This integration produces the same Hankel function at this special point, i.e. the coordinate difference of the sinc function's peak. This property provides us not using the integral but a functional expression with the specified error criteria and hence the running time of the code reduces appreciably. The relative error in the computation of the main matrix elements reduces to zero as the bandwidth of the spatial domain sinc function increases to infinity. Our computation revealed that acceptable accuracy is obtained in reasonable bandwidth. The error is tabulated and presented in the numerical results section.

2. Formulation

Geometry with the general multi N strip case is illustrated in Figure 1(a). We use a finite set of parallel conducting strips, infinitely long in the y-direction, located in the $z = 0$ plane. Coordinates of the initial and final points of the strips are $(x_{i1}, 0)$ and $(x_{i2}, 0)$ for the i^{th} strip, where $i = 1,2,\ldots,N$. This N strip geometry is illuminated by the incident field with angle θ^{inc} with the z-axis. The time dependence e^{jwt} will be suppressed throughout.

The integral equation (IE) here can be derived by imposing the boundary conditions on the conducting parts. The problem is formulated for both E and H polarities. Also, the scatterer surface is sampled uniformly for the entire conducting part of the grating surface.

We thus separately examine the E-polarization and H-polarization cases.

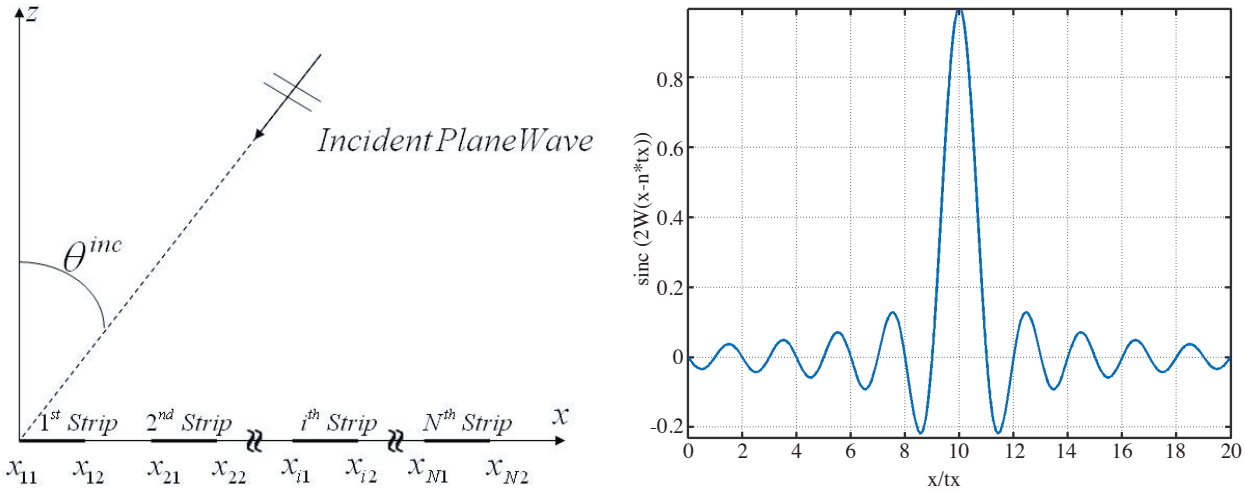

Figure 1. (a) Geometry of the problem for general N strip case (b) The sinc function given in the rectangular coordinate system. The parameters of the sinc geometry can be written that n=10, W=500 and tx=0.001.

2.1. E-polarization case

The integral equation for the E-polarization can be given

$$E_y^{in}(x) = -(\omega\mu/4)\sum_{i=1}^{N}\int_{x_{i1}}^{x_{i2}} J_y^i(x')\, H_0^{(2)}(k|x-x'|)\, dx' \tag{1}$$

where x is in the direction of the conducting parts of the strips. Equation (1) can be obtained by using the auxiliary vector and scalar potentials. However, here there is no $y$variation in the 2D geometry. Therefore the derivatives with respect to y drop and the auxiliary vector potential simply produces equation (1). The surface current density $J_y^i(x')$can be expanded into N dimensional orthogonal functional space consisting of sinc type basis functions (see Appendix A). The surface current on the i^{th} strip is given via the surface current density with a sampling frequency $1/(2W)$ (see Figure 1(b))

$$J_y^i \cong \sum_{p(i)=n_{i1}}^{n_{i2}} x_{p(i)}\mathrm{sinc}(2Wx' - p(i)), \tag{2}$$

where W is the bandwidth of the sinc function and $x_{p(i)}$ is the unknown coefficients of the current density on the i^{th} strip. Also, $n_{i1}\, t_x = x_{i1}$ and $n_{i2}\, t_x = x_{i2}$, where $t_x = 1/(2W)$. Hence numbers n_{i1} and n_{i2} correspond to the initial and final sampling points of the i^{th} strip and $p(i)$ defining the points on the i^{th} strip between n_{i1} and n_{i2}. The expanded current is substituted into the original integral equation in (1). Then by testing it with the same type sinc functions gives the following equation.

$$\begin{gathered}\int_{-\infty}^{\infty} E_y^{in}(x)\mathrm{sinc}(2Wx - m(j))dx = -\tfrac{\omega\mu}{4}\sum_{i=1}^{N}\sum_{p(i)=n_{i1}}^{n_{i2}} x_{p(i)}\int_{-\infty}^{\infty}\mathrm{sinc}(2Wx - m(j))dx \\ \int_{-\infty}^{\infty}\mathrm{sinc}(2Wx' - p(i))H_0^{(2)}(k|x-x'|)dx' \quad j = 1, 2, \ldots, N\end{gathered} \tag{3}$$

where $m(j)$ define the points of the j^{th} strip. As the bandwidth in the frequency domain W is assumed to be large, then the integral limits of the sinc function in spatial domain (i.e beam width) reduces to small

values. We only consider the peak values of the sinc functions in a given position (i.e. basis functions), and by taking the integrals from minus to plus infinity with small error criteria like a generalized function. Defining a new variable u as $u = x - x\prime$, equation (3) can be modified and written as

$$\begin{array}{c} \int_{-\infty}^{\infty} E_y^{in}(x)\mathrm{sinc}(2Wx - m(j))dx = -\frac{\omega\mu}{4}\sum_{i=1}^{N}\sum_{p(i)=n_{i1}}^{n_{i2}} x_{p(i)} \int_{-\infty}^{\infty} H_0^{(2)}(k\,|u|) \\ \left(\int_{-\infty}^{\infty}\mathrm{sinc}(2Wx - m(j))\,\mathrm{sinc}(2W(x-u) - p(i))dx\right)du \end{array} \tag{4}$$

where the inner integral states the convolution of two sinc functions; and by using the property of the convolution of two sinc function (see Appendix B), we can write the above equation as

$$E_y^{in}(m(j)t_x) = -\frac{\omega\mu}{4}\sum_{i=1}^{N}\sum_{p(i)=n_{i1}}^{n_{i2}} x_{p(i)}\int_{-\infty}^{\infty}\mathrm{sinc}(2Wu + p(i) - m(j))H_0^{(2)}(k|u|)du \tag{5}$$

$j = 1, 2, \ldots, N$ where $m(j)$ and $p(i)$ are the integer numbers on the i^{th} and j^{th} strips, respectively, with the properties $x_{j1} \le m(j)\,t_x \le x_{j2}$ and $x_{i1} \le p(i)\,t_x \le x_{i2}$. The left hand side of equation (5) comes from the complete orthogonal expansion of the function $E_y^{in}(x)$ and the orthogonal property of the sinc function (see appendix A).

The above algebraic equation can be put into the following matrix equation by considering a specified low error (see section 3)

$$[A_{mp}^{ji}][x_{pi}] = [B_m^j] \tag{6}$$

where

$$A_{mp}^{ji} = \begin{cases} t_x\; H_0^{(2)}(k\,t_x|m(j) - p(i)|) & m(j) \neq p(i) \\ \int_{-\infty}^{\infty}\mathrm{sinc}(2Wu)\; H_0^{(2)}(k|u|)\,du & elsewhere \end{cases} \tag{7}$$

and

$$B_m^j = E_y^{inc}(m(j)t_x) \tag{8}$$

The integral property of the sinc function is used in the derivation of equations (7). The details on this property are given in the next section.

2.2. H polarization case

By the aids of auxiliary potentials, the integral equation for H polarization can be given as

$$E_x^{in}(x) = \frac{\omega\mu}{4}\sum_{i=1}^{N}\int_{x_{i1}}^{x_{i2}} J_x^i(x')H_0^{(2)}(k|x-x'|)dx' + \frac{1}{4\omega\varepsilon}\frac{\partial}{\partial x}\sum_{i=1}^{N}\int_{x_{i1}}^{x_{i2}}\frac{\partial J_x^i(x')}{\partial x'}H_0^{(2)}(k|x-x'|)dx'. \tag{9}$$

Equation (9) is derived by using auxiliary vector and scalar potentials and in the auxiliary scalar potential the unknown is the charge density function ρ. But it can be expressed by the divergence of the current density function using the equation of the continuity i.e. $\rho = (\frac{1}{j\omega})\nabla\cdot\vec{J}$. In this equation, derivative of variable x in the second part of the integral equation can be applied directly to Green's function, i.e. Hankel

function. Then this derivative can be transformed onto the current function by integration by parts. The integral equation can then be modified to

$$\begin{aligned} E_x^{in}(x) = \tfrac{\omega\mu}{4}\sum_{i=1}^{N}\int_{x_{i1}}^{x_{i2}} J_x^i(x')H_0^{(2)}(k|x-x'|)dx' - \tfrac{1}{4\omega\varepsilon}\sum_{i=1}^{N}\left\{\tfrac{\partial J_x^i(x')}{\partial x'}H_0^{(2)}(k|x-x'|)\right\}\Big|_{x'=x_{i1}}^{x'=x_{i2}} \\ +\tfrac{1}{4\omega\varepsilon}\sum_{i=1}^{N}\int_{x_{i1}}^{x_{i2}}\tfrac{\partial^2 J_x^i(x')}{\partial x'^2}H_0^{(2)}(k|x-x'|)dx' \end{aligned} \tag{10}$$

The first order derivatives of the $J_x^i(x')$in the second term of (10) can be computed by the finite difference approximation.

$$\left.\frac{\partial J_x^i(x')}{\partial x'}\right|_{x'=x_{i1}} = \frac{J_x^i((n_{i1}+1)t_x) - J_x^i(n_{i1}t_x)}{t_x} \cong J_x^i((n_{i1}+1)t_x)/t_x \tag{11}$$

$$\left.\frac{\partial J_x^i(x')}{\partial x'}\right|_{x'=x_{i2}} = \frac{J_x^i(n_{i2}t_x) - J_x^i((n_{i2}-1)t_x)}{t_x} \cong -J_x^i((n_{i2}-1)t_x)/t_x \tag{12}$$

Also, $J_x^i(n_{i2}t_x)$ and $J_x^i(n_{i1}t_x)$ are zero parameters, since no normal current flows at the edges. Then

$$\begin{aligned} E_x^{in}(x) = \tfrac{\omega\mu}{4}\sum_{i=1}^{N}\int_{x_{i1}}^{x_{i2}} J_x^i(x')H_0^{(2)}(k|x-x'|)dx' \\ +\tfrac{1}{4\omega\varepsilon}\sum_{i=1}^{N}\tfrac{J_x^i((n_{i1}+1)t_x)}{t_x}H_0^{(2)}(k|x-x_{i1}|) \\ +\tfrac{1}{4\omega\varepsilon}\sum_{i=1}^{N}\tfrac{J_x^i((n_{i2}-1)t_x)}{t_x}H_0^{(2)}(k|x-x_{i2}|) \\ +\tfrac{1}{4\omega\varepsilon}\sum_{i=1}^{N}\int_{x_{i1}}^{x_{i2}}\tfrac{\partial^2 J_x^i(x')}{\partial x'^2}H_0^{(2)}(k|x-x'|)dx' \end{aligned} \tag{13}$$

The surface current density $J_x^i(x')$can be expanded as before into the sinc type orthogonal basis functions (see Appendix A). The surface current density on the i^{th} strip is specified as (see Figure 1(b))

$$J_x^i(x') = \sum_{p(i)=n_{i1}+1}^{n_{i2}-1} x_{p(i)}\mathrm{sinc}(2Wx'-p(i)). \tag{14}$$

Substituting equation (14) into the equation (13), and also considering the surface current as the combination of the closely sampled points on the scatterer surface, the second derivative of the current density, i.e. $\frac{\partial^2 J_y}{\partial x^2}$, can be taken as a second-order finite difference equation. We thus obtain the relation

$$\begin{aligned} E_x^{in}(x) \cong \tfrac{\omega\mu}{4}t_x\sum_{i=1}^{N}\sum_{p(i)=n_{i1}+1}^{n_{i2}-1} x_{p(i)}\int_{-\infty}^{\infty}\mathrm{sinc}(2Wx'-p(i))H_0^{(2)}(k|x-x'|)dx' \\ +\tfrac{1}{4\omega\varepsilon}\sum_{i=1}^{N}\tfrac{x_{(n_{i2}-1)}}{t_x}H_0^{(2)}(k|x-x_{i2}|) \\ +\tfrac{1}{4\omega\varepsilon}\sum_{i=1}^{N}\tfrac{x_{(n_{i1}+1)}}{t_x}H_0^{(2)}(k|x-x_{i1}|) \\ +\tfrac{1}{4\omega\varepsilon}t_x\sum_{i=1}^{N}\sum_{p(i)=n_{i1}+1}^{n_{i2}-1}\tfrac{[x_{(p(i)+1)}-2x_{p(i)}+x_{(p(i)-1)}]}{t_x^2}\int_{-\infty}^{\infty}\mathrm{sinc}(2Wx'-p(i))\ H_0^{(2)}(k|x-x'|)dx' \end{aligned} \tag{15}$$

Residual error obtained from equation (15) will be minimized by testing it with the sinc-type testing functions in the N dimensional orthogonal functional space. This is the original method of moments procedure (referred as the Galerkin procedure). The following equation can then be obtained using the procedure given in the E-polarization case (by considering the property that the convolution of two sinc functions is also a sinc function, as given in Appendix B).

$$\begin{aligned}\int_{-\infty}^{\infty} E_x^{in}(x)\mathrm{sinc}(2Wx-m(j))dx &= \tfrac{\omega\mu}{4}t_x\sum_{i=1}^{N}\sum_{p(i)=n_{i1}+1}^{n_{i2}-1} x_{p(i)}\int_{-\infty}^{\infty}\mathrm{sinc}(2Wu-m(j)+p(i))H_0^{(2)}(k|u|)du\\
&+\tfrac{1}{4\omega\varepsilon}\sum_{i=1}^{N}\tfrac{x_{(n_{i2}-1)}}{t_x}\int_{-\infty}^{\infty}\mathrm{sinc}(2Wu-m(j))H_0^{(2)}(k|u-x_{i2}|)du\\
&+\tfrac{1}{4\omega\varepsilon}\sum_{i=1}^{N}\tfrac{x_{(n_{i1}+1)}}{t_x}\int_{-\infty}^{\infty}\mathrm{sinc}(2Wu-m(j))H_0^{(2)}(k|u-x_{i1}|)du\\
&+\tfrac{1}{4\omega\varepsilon}t_x\sum_{i=1}^{N}\sum_{p(i)=n_{i1}+1}^{n_{i2}-1}\tfrac{[x_{(p(i)+1)}-2x_{p(i)}+x_{(p(i)-1)}]}{t_x^2}\int_{-\infty}^{\infty}\mathrm{sinc}(2Wu-m(j)+p(i))H_0^{(2)}(k|u|)du\\
&\qquad\qquad j\ =\ 1,2,\ldots,N\end{aligned} \tag{16}$$

Equation (16) can also be written as follows by defining the matrix elements

$$\begin{aligned}B_m^j =\ & \tfrac{\omega\mu}{4}\,t_x\sum_{i=1}^{N}\sum_{p(i)=n_{i1}+1}^{n_{i2}-1} x_{p(i)}\,A_{pm}^{ji}\ +\ \tfrac{1}{4\omega\varepsilon t_x}\sum_{i=1}^{N} x_{n_{i2}-1}D_m^{ji}+\tfrac{1}{4\omega\varepsilon t_x}\sum_{i=1}^{N} x_{n_{i1}+1}C_m^{ji}\\
&+\ \tfrac{1}{4\omega\varepsilon t_x}\sum_{i=1}^{N}\sum_{p(i)=n_{i1}+1}^{n_{i2}-1}\left(x_{p(i)+1}-2x_{p(i)}\ +\ x_{p(i)-1}\right)\,A_{pm}^{ji}\end{aligned} \tag{17}$$

where A_{pm}^{ji}, C_m^{ji} and D_m^{ji} and are given in the final equations of this section. In the above algebraic matrix equation, the second and third terms constitute the column matrices but the last term can be modified by shifting to left and right depending on the indices under the x parameter that are the unknown coefficients of the current density. Then assuming $p(i)+1=u$ and $p(i)$-$1=v$, and then by using a change of variable, we constitutes the F_{ji} and G_{ji} matrices where the first and last columns are produced by C_m^{ji}, D_m^{ji} column matrices, respectively. The middle part of the last term in the equation (17) is the similar to the first term produced by A_{ji}. After these modifications, the matrix equation can be given as

$$\begin{aligned}\begin{bmatrix} B_1\\ B_j\\ B_N\end{bmatrix} &= \tfrac{\omega\mu}{4}t_x\begin{bmatrix} A_{11} & \ldots\ldots & A_{1N}\\ A_{ji} & & \\ A_{N1} & \ldots\ldots & A_{NN}\end{bmatrix}\begin{bmatrix} x_1\\ x_i\\ x_N\end{bmatrix}-\tfrac{2}{4\omega\varepsilon}\tfrac{1}{t_x}\begin{bmatrix} A_{11} & \ldots\ldots & A_{1N}\\ A_{ji} & & \\ A_{N1} & \ldots\ldots & A_{NN}\end{bmatrix}\begin{bmatrix} x_1\\ x_i\\ x_N\end{bmatrix}\\
&+\tfrac{1}{4\omega\varepsilon}\tfrac{1}{t_x}\left\{\begin{bmatrix} F_{11} & \ldots\ldots & F_{1N}\\ F_{ji} & & \\ F_{N1} & \ldots\ldots & F_{NN}\end{bmatrix}\begin{bmatrix} x_1\\ x_i\\ x_N\end{bmatrix}+\begin{bmatrix} G_{11} & \ldots\ldots & G_{1N}\\ G_{ji} & & \\ G_{N1} & \ldots\ldots & G_{NN}\end{bmatrix}\begin{bmatrix} x_1\\ x_i\\ x_N\end{bmatrix}\right\}\end{aligned} \tag{18}$$

where i and j vary between 1 and N and each A_{ji} has a rectangular matrix form in the matrix size of the $Q_2\times Q_1$, B_j has the column matrix size Q_2 and x_i has the matrix size Q_1. Also matrices A_{ji} and B_j have

the form

$$A_{ji} = \begin{bmatrix} A_{11}^{ji} & A_{12}^{ji} & .. & A_{1Q_1}^{ji} \\ . & & & \\ . & & & \\ A_{Q_2 1}^{ji} & A_{Q_2 2}^{ji} & .. & A_{Q_2 Q_1}^{ji} \end{bmatrix}_{Q_2 x Q_1} \quad and \quad B_j = [B_1\, B_2 \ldots\, B_{Q_2}], \tag{19}$$

where Q_2 and Q_1can be given as $Q_2 = n_{j2} - n_{j1}$-1 and $Q_1 = n_{i2} - n_{i1}$-1. Matrices F_{ji} and G_{ji} can be constructed by using C and D column matrices in the first and last columns of the F_{ji} and G_{ji} matrices, respectively.

$$F_{ji} = \left[\begin{array}{c|ccc} C_1^{ji} & A_{11}^{ji}. & A_{(p-1)1}^{ji}. & A_{(Q_1-1)1}^{ji} \\ \vdots & \vdots & \vdots & \vdots \\ C_m^{ji} & A_{1m}^{ji}. & A_{(p-1)m}^{ji}. & A_{(Q_1-1)m}^{ji} \\ \vdots & \vdots & \vdots & \vdots \\ C_{Q_2}^{ji} & A_{1Q_2}^{ji}. & A_{(p-1)Q_2}^{ji}. & A_{(Q_1-1)Q_2}^{ji} \end{array}\right]_{Q_2 x Q_1} \tag{20a}$$

$$G_{ji} = \left[\begin{array}{ccc|c} A_{21}^{ji}. & A_{(p+1)1}^{ji}. & A_{(Q_1-1)1}^{ji} & D_1^{ji} \\ \vdots & \vdots & \vdots & \vdots \\ A_{2m}^{ji}. & A_{(p+1)m}^{ji}. & A_{(Q_1-1)m}^{ji} & D_m^{ji} \\ \vdots & \vdots & \vdots & \vdots \\ A_{2Q_2}^{ji}. & A_{(p+1)Q_2}^{ji}. & A_{(Q_1-1)Q_2}^{ji} & D_{Q_2}^{ji} \end{array}\right]_{Q_2 x Q_1} \tag{20b}$$

Here, column matrices C and D are defined as

$$C_m^{ji} = \int_{-\infty}^{\infty} \sin c(2Wx - m(j)) H_0^{(2)}(k|x - x_{i1}|)dx \tag{21a}$$

$$D_m^{ji} = \int_{-\infty}^{\infty} \sin c(2Wx - m(j)) H_0^{(2)}(k|x - x_{i2}|)dx \tag{21b}$$

The source column matrix B is the combination of the B_j matrices each having the size of Q_2 matrix. Elements of B matrix elements can be found by using simple sampling the points i.e. the points $m(j)$ on the strip j as such

$$B_m^j = t_x E_x^{in}(t_x m(j)) \ . \tag{22}$$

Also main matrices A_{ji} are combinations of the different rectangular matrices with sizes of $Q_2\ xQ_1$.

The main matrix and the other C_m^{ji} and D_m^{ji} matrices can be computed in a reasonable cpu times through the properties of the sinc function. In this computation, the error criteria can be specified and studied in the next section. The main matrix elements can be given as

$$A_{mp}^{ji} = \int_{-\infty}^{\infty} \mathrm{sinc}(2Wu - m(j) + p(i)) H_0^{(2)}(k|u|)du. \tag{23}$$

The resultant convolution function of the given two sinc functions for observation and source points is $\mathrm{sinc}(2\,Wu\text{-}m + p)$. Notice that the location of the new sinc function is defined as $m - p$. Time consuming evaluation for a new analytical sub domain function is not required.

This new sinc function near the Hankel function can be computed as given in the next section in the equation (24), with specified low error criteria. Therefore no extra integration cost is required but the discretization level of the scatterer has to be large compared to the ordinary MoM.

3. Approximate Evaluation of the Sinc Integrals

For the matrix elements given above, we compute the integrals of the sinc function with a tuned error criteria. The integral identity can be written as

$$\int_{-\infty}^{\infty} \mathrm{sinc}(2Wu - m + p)\, H_0^{(2)}(k|u|)\, du \;=\; t_x\, H_0^{(2)}(k\,|m-p|\,t_x) \;+\; Error, \tag{24}$$

where m, p and L(small) are integer numbers and $|p-m| \geq L$. Also, if $|p-m| < L$, then the integrals are numerically taken without any problem. Because the Hankel function has only logarithmic singularity. This means that it is a kind of numerically integrable function. W is the bandwidth of the spatial domain sinc function in the frequency domain counterpart. (Recall that t_x=$1/(2W)$). Here, the sinc function is integrated with the appearing the zero order and second kind Hankel function in the same integrand. The aim is to approximate the sinc integral with the simple Hankel function written in the right hand side of the equation (24). However this equation can be satisfied if the error function is very small compared to the value of the original sinc integral in the equation (24).

To find an approximate function for our error criteria, one can apply Parseval's relation to both sides of the equation (24). Then in the frequency domain, the left hand side has a finite integral and the right hand side has the infinite integral having the same integrand. The difference between two parts of the main integrals in the frequency domain gives us the error function. This error function can be written as

$$Error = t_x \int_{W}^{\infty} \frac{4}{\sqrt{k^2 - 4\pi^2 f_x^2}}\, \cos\, \frac{\pi f_x (p-m)}{W}\, df_x, \tag{25}$$

where f_x is the spectral domain parameter which is the frequency domain counterpart of the spatial domain range. Equation (25) can be converted (within the high frequency limit, i.e. $4\pi^2 \mathrm{f}_x^2 \;\; >> \mathrm{k}^2$) to the form

$$Error \cong -\frac{i}{\pi W} \int_{\pi|(p-m)|}^{\infty} \frac{\cos u}{u}\, du, \tag{26}$$

where $\cos(u)/u$ is a special tabulated function i.e. $\mathrm{Ci}(z)$. Thus we have absolute error as

$$Error \cong \frac{i}{\pi W}\, Ci(\pi|(p-m)|). \tag{27}$$

We note that integral (24) can be approximated simply by Hankel function as defined in the right hand side of equation (24), if p is not close to m. If this equality holds, i.e. p close to m (near diagonal elements), then the integral can be numerically evaluated. In general, the maximum error occurs when $p - m = L$, where L=0 and the relative value of this error is tabulated in Table 1. If L becomes larger, i.e. L >1, the relative error decreases (see Table 1).

4. Numerical Results

Our numerical results are presented for the general geometry given in Figure 1(a) and its three strip special case is also considered, using the formulation given in the previous sections. Surface current density

distributions induced on the strips are obtained as the plane electromagnetic wave illuminates the strips. Our aim is to make computations in reasonable cpu times, and even reduce cpu time when treating reradiating characteristics. We achieve this by exploiting the properties of the sinc functions.

Table 1. Relative error of the computed main integral.

Bandwidth W, parameter t_x and sample point number N per λ (λ=0.06 m)	Relative Error in the Computational Process of the main matrix elements for L=1 $\left\lvert \frac{Ci(L\pi)}{\pi W} \frac{1}{t_x H_0^{(2)}(kLt_x)} \right\rvert$	Relative Error in the Computational Process of the main matrix elements for L=2 $\left\lvert \frac{Ci(L\pi)}{\pi W} \frac{1}{t_x H_0^{(2)}(kLt_x)} \right\rvert$
W=208.3(1/m), N=25 and tx=0.04λ	0.0353	0.0142
W=416.6(1/m), N=50 and tx=0.02λ	0.0280	0.0109
W=833.3(1/m), N=100 and tx=0.01λ	0.0229	0.0086
W=4166.6(1/m), N=500 and tx=0.002λ	0.0158	0.0056
W= 8333.3(1/m), N=1000 and tx=0.001λ	0.0138	0.0048

Simulations were carried out on an AMD Athlon 3200+ 2.0 GHz processor with 1.00 GB RAM under Matlab®7.0 program package on the windows operating system. This is readily available through a desktop code to compute the problem with a sinc basis functions in reasonable cpu times. Since the computation time depends on the total number of basis functions and increasing the bandwidths of sinc functions causes also the increase in the number of sample points on the strips. In the simulations, the number of points (for example like N=50 points and W=416.6 (1/meter) see table 1 and II) is selected to evaluate matrix elements in the reasonable time with a low error rate. This technique is applied to the general geometry in Figure1 (a) by considering N=10 and N=3 strip cases. . The geometry is divided into equally spaced sample points and uniform meshing is applied to the conducting surface parts. MoM procedure is used to calculate the current densities on the strips. We have analyzed both TE and TM modes of incident wave and plotted for various angles of incidence.

First, we examined here horizontal strips equally spaced in free space in Figure 1(a). The parameters are set when producing Figure 2, the width of the strips as $(1/\pi)\lambda$ and the spacing between the strips as $(1/\pi)\lambda$. We fixed the total number of strips N=10, but W will be determined depending on the number basis (sinc) functions on each strip. The magnitude and the phase of the current densities on the strips are shown in Figure 2 and Figure 3, respectively, for both TE and TM mode excitations. Forty sinc functions per strip is chosen for TE case and this is equivalent to W=1046.6 $(\text{meter})^{-1}$. The number of basis functions whereas 160 per strip for TM case and this is equivalent to W=4180.6 $(\text{meter})^{-1}$.

Simulations for various values of the strip widths and the spacing between the strips have been carried out and the results are compared with the results of [15, 16]. In Figure 2 and Figure 3, strip width is fixed. In addition, we get a cpu processing reasonable. Figure 2 and Figure 3 shows the current density distributions as a function of normalized length x/λ. Current density distributions induced on the strips are shown in the presence of TM and TE excitations.

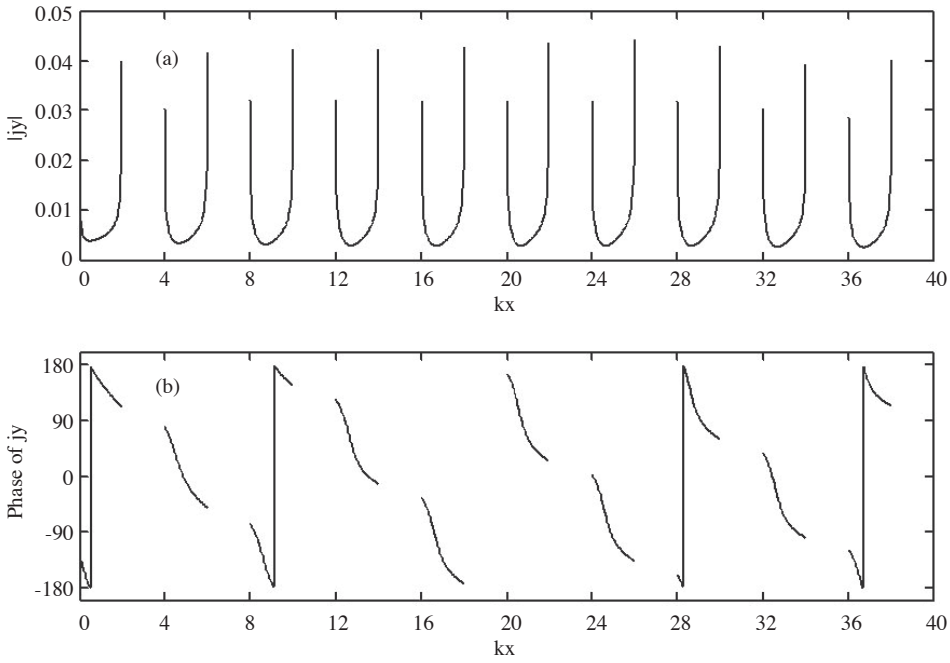

Figure 2. The magnitude and the phase of the surface induced current for 10 strips for parts (a) and (b), respectively. For the TE case, problem parameters are. kw=2, kd=2, N=10 and θ^{inc}=-45°.

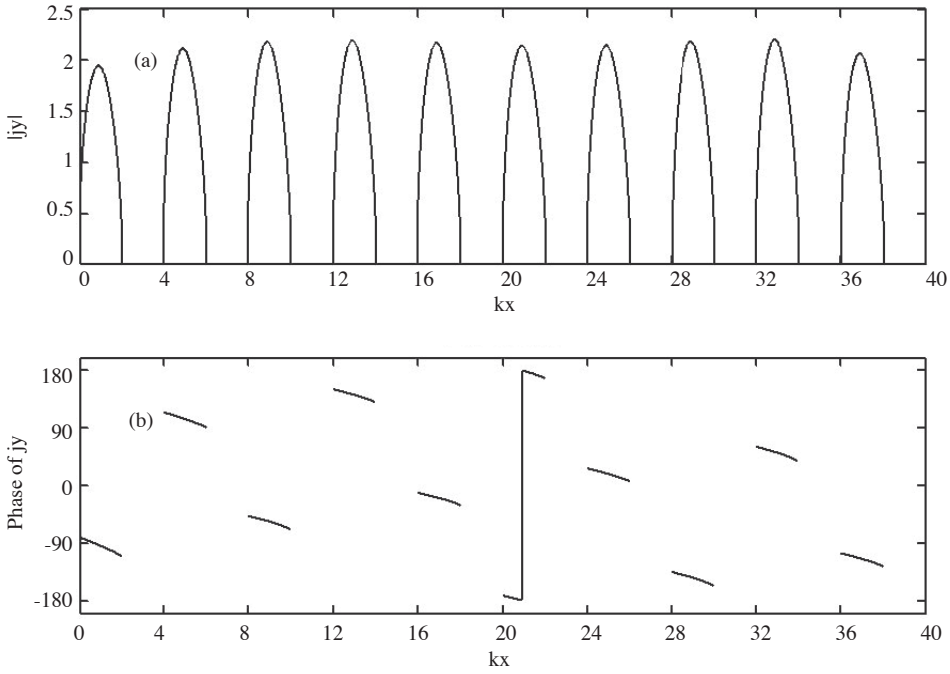

Figure 3. The magnitude and the phase of the surface induced current for 10 strips for parts (a) and (b) respectively. That is the TM case and the problem parameters are. kw=2, kd=2, N=10 and θ^{inc}=-45°.

The second geometry, three horizontal strips separated with $\lambda/2$ distance in free space, is examined as a special case of Figure 1(a) (Each strip has 2λ width) and it is illuminated by plane electromagnetic wave. Parameters for making Figure 4 are chosen as W=290 (meter)$^{-1}$, the number of sinc functions N=70 per

strip for TM case and for Figure 5, W=208 (meter)$^{-1}$, N=50 per strip for TE case. Normal incidence is chosen for both TM and TE cases. The same three strip geometry is also simulated by the ordinary MoM i.e. pulse basis for E-polarization and triangular basis for H-polarization case. Ordinary MoM imposes the analytical convolution between sub domain basis and testing functions; the resultant new function is integrated with a given Hankel type kernel. So more cpu time is required in the ordinary MoM then the sinc-based MoM. The results are plotted on the same graph for both polarizations separately; the real and imaginary parts of current densities are given in Figure 4 and Figure 5. For each case, excellent agreement is observed with the ordinary MoM.

Computation time for the TE case in each geometry is greater than that of the TM case. Since the TE formulation of the geometry is more complicated, more time is consumed to obtain results. In the TM case, magnitude of the current density increases at the endpoints of the strips. It is seen that using our method, such abrupt changes in current density can be well reproduced.

Once current densities are computed, the far field scattering patterns can be obtained depending on the presented formulation. In the Figure 6(a), the scattered field pattern of the current density for the TE excitation of five strips is given. For the TM case given in Figure 6(b), the following parameters are chosen. the width of the strips is 0.1λ, and the spacing of the strips (d) is 0.4λ. Normalized far field pattern is plotted when incidence angle θ=60°. Figure 6(a) and 6(b) present the agreement with the plots given in [11] for the same geometry. The results show the known facts of the antenna and the theory of the scattering. It can be said that the field does not drop zero on the direction of the x-axis for E-polarization but it drops the zero for the H-polarization case.

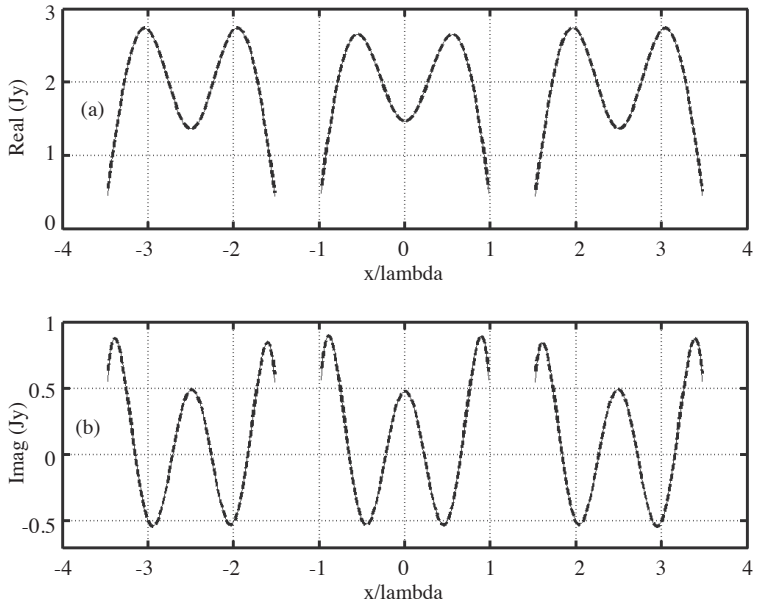

Figure 4. The magnitude of the surface induced current for 3 strips. That is the TE case and N=3, θ^{inc}=0°. Each strip has 2λ width and 0.5λ distance between the strips. Figures (a) and (b) are the real and imaginary parts of the current densities respectively. Solid line shows the sinc-based MoM; and the dashed line shows the pulse-type ordinary MoM solution.

For the three strip special geometry, not the relative error of the whole problem but the relative error of the computed main integral in the formulation is tabulated in Table 1. Relative error for different tx values

are presented via the Ci function table. It is observed that as tx increases or W decreases, the relative error increases. Relative error reached 0.01 value when W=416.6 (meter)$^{-1}$ and the number of basis functions was taken as N=50 at L=2 case (Table 1). In Table 1, the number of basis functions are chosen first and then the other parameters tx and W are obtained. In theory increasing W gives more accurate results. But in reality for reasonable W values results can be produced within acceptable error limits. The relative error in the computation of the main integrals can be reduced by taking L>1. The error level of the main integrals is in the same status of the accuracy of the ordinary MoM.

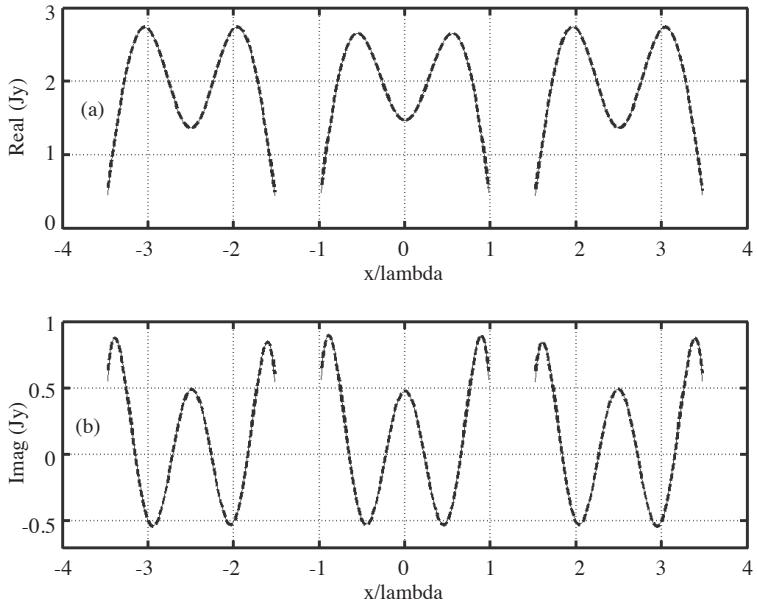

Figure 5. The magnitude of the surface induced current for 3 strips. That is the TM case and N=3, θ^{inc}=0°. Each strip has 2λ width and 0.5λ distance between the strips. Figures (a) and (b) are the real and imaginary parts of the current densities, respectively. Solid line shows the sinc-based MoM and dashed line shows the triangular-type ordinary MoM solution.

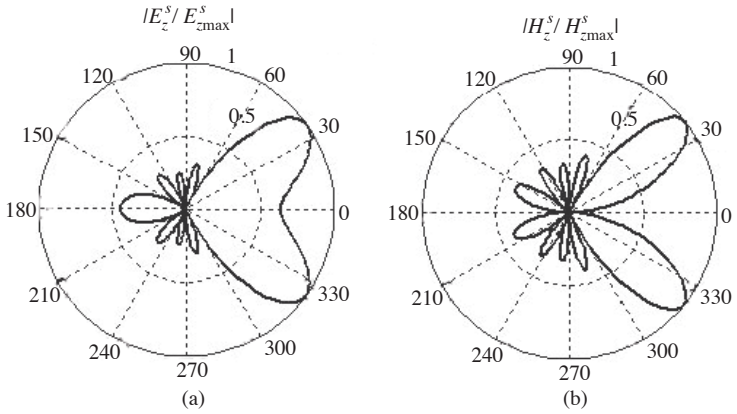

Figure 6. The normalized far field pattern of the scattering radiation for 5 strip case which θ^{inc}=60°. (a) TM case (b) TE case.

Table 2 and Table 3 show CPU time of the overall process of our method and ordinary MoM with pulse and triangular basis functions for E and H polarizations respectively. There is an apparent reduction in the overall running time of the program which solves the same geometry by using sinc based MoM. Three strips each with a 2λ width 0.5λ spacing is used for the simulations.

Table 2. For sinc-based MoM. Cpu time of overall process for 3 strips, each with a 2λ width and 0.5λ spacing, for TE and TM excitations.

	CPU time of overall program, for a 3-strip case, each strip with width 2λ, in seconds (Geometry. Figure1(b)). Sinc type basis functions in MoM.	
Number of sample points on each strip (per 2 lambda)	TE(H-pol)	TM(E-pol)
101	293	12.25
81	138	6.87
61	53	4.23
41	23	2.5

Table 3. For pulse and triangular-based MoM. Cpu time of overall process for 3 strips, each with a 2λ width and 0.5λ spacing, for TE and TM excitations.

	CPU time of overall program, for a 3-strip case, each strip with width 2λ, in seconds (Geometry. Figure1(b)). Comparison of ordinary pulse (E-pol) and triangle (H-pol) sub domain basis functions cases in MoM.	
Number of sample points on each strip (per 2λ)	TE(H-pol)	TM(E-pol)
100	1667	441.23
80	1132	284.7
60	687.8	161.9
40	337.85	73

5. Conclusion

The MoM procedure is applied to finite planar conducting grating for both polarities. Sinc-type basis and testing functions are chosen in the Galerkin procedure. The properties of the sinc functions explained in the previous sections provide faster computation of the main matrix elements over other methods [15, 16]. One useful property of the sinc type basis functions in MoM is to eliminate the analytical convolution between the sub domain basis and testing functions for which a new sinc is enough for this process. This new sinc function is located at the difference points of the source and of the observation. The other exploited property is the integration of the Hankel function with this new sinc function and the result can be approximated by the Hankel function at the points of the source and observation.

These properties used in MoM provide one a fast and an accurate solution in comparison to ordinary MoM. We have shown that without very large W, reasonable accuracy can be obtained.

The sinc based MoM can also be applied numerically to difficult electromagnetic scattering problems, as in 3D geometries. The simplicity of the producing main matrix elements in planar geometries creates the high motivation and the properties of the sinc also the reason of the benefit for using sinc-based MoM.

Appendix A

The set of the sinc functions which are defined in the figure 2 constitutes complete orthogonal set and this orthogonally can be represented as

$$\int_{-\infty}^{\infty} \mathrm{sinc}(2Wx-n)\mathrm{sinc}(2Wx-m)dx = \begin{cases} 1/(2W)\ if\ n=m \\ 0\ if\ n\neq m \end{cases} \tag{28}$$

where n and m are integer numbers and W is the frequency domain bandwidth of the given sinc function originally in the spatial domain. The details of this orthogonally are given in the [19].

Appendix B

The convolution of two sinc functions located at different points in the spatial domain produces a sinc function located at the point of their difference.

$$\int_{-\infty}^{\infty} \underbrace{\mathrm{sinc}(2Wx'-n)}_{g_1(x')}\ \underbrace{\mathrm{sinc}(2W(x-x')-m)}_{g_2(x'-x)}\,dx' = (1/(2W))\ \underbrace{\mathrm{sinc}(2Wx-n+m)}_{g_3(x)}, \tag{29}$$

where n and m are integer numbers and W is the bandwidth of these sinc functions. Equation (23) can also be written as

$$g_1(x) * g_2(-x) = (1/(2W))\, g_3(x). \tag{30}$$

Proof of this relation follows by taking the Fourier transform of both sides.

Acknowledgement

We would like to express our deep gratitude to Prof. Dr. İbrahim Avgin for his suggestions and to improve the English of the written text.

References

[1] R.C. Hall, R. Mittra, "Scattering from a periodic array of resistive strips," IEEE Transactions on AP Vol. 33, No. 9, 1985.

[2] D. Shively, "Scattering from perfectly conducting and resistive strips ona grounded dielectric slab," IEEE Transactions on AP Vol. 42, No. 4, 1994.

[3] L. Carin, L.B. Felsen "Efficient analytical-numerical modeling of ultra-wideband pulsed plane wave scattering from a large dielectric grating," Int. Jour. Of Numerical Modeling. elec. net., devices and fields Vol. 6, pp. 3–17, 1993.

[4] B. Popovski, B. Spasenovski, "Efficient moment method for ultra-wideband scattering from finite array of perfectly conducting and resistive strips on grounded dielectric slab," International Symposium of IEEE 1996, pp. 1406–1409.

[5] T. Ojima, "Absorbtion analysis of a strip grating placed absorber by the method of moments," International Symposium of IEEE 1999, pp. 214–216.

[6] P. Baccarelli, P. Burghignoli, F. Frezza, A. Galli, P. Lamparjello, G. Lovat, S. Paulotto, "Modal properties of surface and leaky waves propagating at arbitrary angles along a metal strip grating on a grounded slab," IEEE Transactions on AP Vol. 53, No. 1, January 2005.

[7] K. Aoki, T. Tonaka, "Diffraction of a plane wave by two parallel conducting plates," Trans. IECE Japan Vol. J60-B, pp. 836–842, 1977.

[8] M. Shimoda, T. Hakura, "Scattering by parallel plates," Radio Science Vol. 22, pp. 987–991, 1987.

[9] W.A. Walker, C.M. Butler,"A method of computing scattering by large arrays of narrow strips," IEEE Trans. AP Vol. 32, pp.1327–1334, 1984.

[10] M. Nishimoto, K. Aoki, "Scattering of electromagnetic plane waves by arbitrarily oriented two parallel conducting strip," IECE Japan Vol. 69-B, pp. 1131–1139, 1986.

[11] A. Matsushima, T. Hakura, "Singular integral equation approach to electromagnetic scattering from a finite periodic array of conducting strips," Journal of Electromagnetic Waves and Applications Vol. 5, No. 6, pp. 545–562, 1991

[12] F. Stenger, Numerical methods based on the sinc and analytic functions, Springer-Verlag, Newyork, 1993.

[13] J. Lund, K. Bowers, Sinc methods for quadrature and differential equations, SIAM, Philadelphia, 1992.

[14] A. Saadatmandi, M. Razzaggi, M. Dehghan, "Sinc-Collocation methods for the solution of Hallen's integral equation," Journal of Electromagnetic Waves and Applications, Vol. 19, No. 2, pp. 245–256, 2005.

[15] M.I. Aksun, F. Çalışkan, L. Gurel, "An efficient method for electromagnetic characterization of 2-D geometries in stratified media" IEEE Trans. On AP Vol. 50 No. 5, 2002.

[16] L.Gurel, W.C. Chew, " A recursive T-matrix algorithm for strips and patches" Radio Sci. vol.27, pp. 387–401, May-June 1992.

[17] E.I. Veliev, V.V. Veremey, "Numerical-Analytical approach for the solution to the wave scattering by polygonal cylinders and flat strip structures" Analytical and Numerical Methods in Electromagnetic Wave Theory, Ch.10, Siance House, Tokyo, 1993.

[18] F. Kuyucuoğlu, Z. Çay, T. Oğuzer "Scattering from the pec flat strip by using the method of moments with sinc type basis functions" Sixth International Conference on Computational Electromagnetics CEM 2006 proceedings, pp. 91–92.

[19] S. Haykin, Communication Systems, pp. 364–370.